Dalton Transactions

ROYAL SOCIETY OF CHEMISTRY

PAPER

View Article Online
View Journal | View Issue

Cite this: *Dalton Trans.*, 2024, **53**, 18983

Development of thiacrown ligands for encapsulation of mercury-197m/g into radiopharmaceuticals†

Parmissa Randhawa, [a,b] Cailum M. K. Stienstra, [b] Shaohuang Chen, [a,b] Yang Gao, [c,d] Georg Schreckenbach, [c] Valery Radchenko[b,e] and Caterina F. Ramogida *[a,b]

The theranostic pair mercury-197m and mercury-197g ($^{197m/g}$Hg, $t_{1/2}$ = 23.8 h/64.14 h), through their γ rays and Meitner–Auger electron emissions, have potential use as constituents in radiopharmaceuticals to treat small metastatic tumours. However, the use of this pair of nuclear isomers in radiopharmaceuticals requires the development of suitable [$^{197m/g}$Hg]Hg^{2+} chelators as currently there is a lack of established ligands for radiometals in the field. Herein, this work studies the ^{nat}Hg/$^{197m/g}$Hg coordination of three thiacrown 18-membered N_2S_4 macrocycles with pendant arms of varying chemical "softness". Following the synthesis and characterization of the N_2S_4 ligand series (6,6′-((1,4,10,13-tetrathia-7,16-diazacyclooctadecane-7,16-diyl)bis(methylene))dipicolinic acid (**N_2S_4-Pa**), 7,16-bis(pyridin-2-ylmethyl)-1,4,10,13-tetrathia-7,16-diazacyclooctadecane (**N_2S_4-Py**) and 7,16-bis(2-(methylthio)ethyl)-1,4,10,13-tetrathia-7,16-diazacyclooctadecane (**N_2S_4-Thio**)), Hg^{2+} complexes were studied through mass spectrometry, nuclear magnetic resonance (NMR) spectroscopy, and density functional theory (DFT) calculations, revealing successful complexation of all ligands with the Hg^{2+} ion. Radiolabeling studies demonstrated the effect of the pendant arm on [$^{197m/g}$Hg]Hg^{2+} coordination, as **N_2S_4-Thio** and **N_2S_4-Py** had the highest radiochemical yield, similar to that of previously reported *N*-benzyl-2-(1,4,7,10-tetrathia-13-azacyclopentadecan-13-yl) acetamide (**NS_4-BA**), while **N_2S_4-Pa** had the lowest. The complex integrity of [$^{197m/g}$Hg]**[Hg(N_2S_4-Py)]$^{2+}$** and [$^{197m/g}$Hg]**[Hg(N_2S_4-Thio)]$^{2+}$** in both human serum and glutathione was notably lower compared to the [$^{197m/g}$Hg][Hg(**NS_4-BA**)]$^{2+}$ complex. However, the [$^{197m/g}$Hg]**[Hg(N_2S_4-Py)]$^{2+}$** and [$^{197m/g}$Hg]**[Hg(N_2S_4-Thio)]$^{2+}$** complexes remained above 70% intact over 82 h when competed against biologically relevant metals ($ZnCl_2$, $FeCl_3$, $CuCl_2$, $MgCl_2$ and $CoCl_2$), suggesting the selectivity of the ligands for Hg^{2+}. This study illustrates the importance of the macrocyclic backbone size and electron-donor groups of the donor pendant arms in the design of chelators for $^{197m/g}$Hg-radiopharmaceuticals, as both affect the radiolabeling properties and complex inertness.

Received 26th August 2024,
Accepted 15th October 2024

DOI: 10.1039/d4dt02427c

rsc.li/dalton

Introduction

Theranostic radiopharmaceuticals in nuclear medicine continue to attract interest as these radioactive drugs have the potential to both image (*via* diagnostic scans) and treat diseases such as cancer (*via* therapeutic radiation) simultaneously in one treatment dose. In particular, mercury-197m and mercury-197g ($^{197m/g}$Hg, $t_{1/2}$ = 23.8 h/64.14 h) are a promising pair of radioactive isomers for incorporation into a chemically matched theranostic agent as they can be used as a diagnostic agent by single-photon emission computed tomography (SPECT) imaging and as a therapeutic *via* decay emissions of gamma rays [^{197m}Hg: 133.98 keV, I = 33.5%] and cytocidal Meitner–Auger electrons (MAEs) [average yield/decay = 42.6], respectively.[1–4] Chemically matched theranostic agents are not only beneficial for the synthesis of radiopharmaceuticals (as both isotopes can use the same chelator) but also beneficial for biodistribution as their chemical structures and charges are identical. Thus, clinicians can accurately monitor the distribution and the therapeutic efficacy of radiopharmaceuticals

[a]*Department of Chemistry, Simon Fraser University, Canada. E-mail: cfr@sfu.ca*
[b]*Life Sciences Division, TRIUMF, Canada*
[c]*Department of Chemistry, University of Manitoba, Canada*
[d]*Institute of Fundamental and Frontier Sciences, University of Electronic Science and Technology of China, China*
[e]*Department of Chemistry, University of British Columbia, Canada*

†Electronic supplementary information (ESI) available: Experimental 1D and 2D; ^{1}H, ^{13}C NMR spectra, mass spectra, DFT data, radio-iTLC chromatograms, labeling and kinetic inertness assay data. See DOI: **https://doi.org/10.1039/d4dt02427c**

via imaging, allowing for the development of personalized treatment options.[2]

One of the key components of an inorganic radiopharmaceutical is the bifunctional chelate (BFC), which joins the radiometal to a biomolecule/targeting vector, allowing for site-specific delivery of the radiopharmaceutical to diseased cells while minimizing the effect of radiation on adjacent tissues.[5] The BFC method is attractive due to the ability to perform all the synthesis of the chelate and biomolecule before the addition of the radionuclide, saving many half-lives of radioactivity.[6] Radiopharmaceuticals require the administration of only trace amounts (ng–pg) of radionuclide, allowing for traditionally toxic metals such as Hg^{2+} to be used for theranostic purposes without concerns of chemical toxicity.[1,7]

Presently, there are few selective and stable chelating ligands suitable for $^{197m/g}$Hg radiopharmaceutical use. Our previous work demonstrated commercial chelators DOTA and DOTAM (aka TCMC) as unsatisfactory for [$^{197m/g}$Hg]Hg^{2+} incorporation.[8] Consequently, our work seeks to develop custom ligands for this exotic radiometal pair that matches the coordination chemistry by considering Pearson's hard–soft acid–base (HSAB) theory.[9] To this end, we developed and identified the sulfur-rich chelator *N*-benzyl-2-(1,4,7,10-tetrathia-13-azacyclopentadecan-13-yl)acetamide (**NS_4-BA**) (Fig. 1) as a suitable candidate to complex the "soft" radiometal ion [$^{197m/g}$Hg]Hg^{2+}.[10] **NS_4-BA** exhibited quantitative complexation of [$^{197m/g}$Hg]Hg^{2+} in 60 min, at 80 °C and 37 °C at a ligand concentration of 10^{-4} M, with the resulting radiometal-complex displaying promising inertness when challenged against human serum and glutathione.[10] In developing a second generation of sulfur-containing macrocyclic chelators, we sought to incorporate an additional pendant arm into our NS_4 ligand backbone to improve encapsulation and shielding of the radiometal from *in vivo* competitors, which we hypothesized would improve the inertness of the radiometal-complex. To do so, alterations to the backbone were made to incorporate an additional amine for pendant arm functionalization, resulting in an increase in the backbone size from a 15- to an 18-membered ring. A derivative of this 18-membered N_2S_4 macrocyclic scaffold alkylated with 7-hydroxyquinoline (**TTBQ**; Fig. 1) was previously studied in the environmental mercury sensing literature and was found to rapidly and selectively chelate Hg^{2+} at sub-μM concentrations within a pH range of 5.5–7.5, attaining an association constant (K_a) of 13 020 ± 520 M^{-1}.[11] Most recently, the N_2S_4 scaffold equipped with picolinic acid arms [6,6′-((1,4,10,13-tetrathia-7,16-diazacyclooctadecane-7,16-diyl)bis (methylene))dipicolinic acid (**N_2S_4-H_2Pa** aka H_2S_4macropa)] was investigated by our groups with intermediate radiometals [^{203}Pb]Pb^{2+}, [^{111}In]In^{3+} and [^{213}Bi]Bi^{3+} and showed success for both [^{111}In]In^{3+} and [^{213}Bi]Bi^{3+} incorporation.[12]

We hypothesize that **N_2S_4-Pa^{2-}** may also have a higher affinity for softer (radio)metals such as Hg^{2+}. Two additional pendant arms have been selected for this study, pyridine and thioether arms, resulting in 7,16-bis(pyridin-2-ylmethyl)-1,4,10,13-tetrathia-7,16-diazacyclooctadecane (**N_2S_4-Py**) and 7,16-bis(2-(methylthio)ethyl)-1,4,10,13-tetrathia-7,16-diazacyclooctadecane (**N_2S_4-Thio**), respectively (Fig. 1). The introduction of pyridyl and thioether pendant arms into the cyclen (N_4) backbone has been demonstrated to exhibit high affinity for intermediate (*e.g.* [^{203}Pb]Pb^{2+} and [^{64}Cu]$Cu^{2+/+}$) and soft (*e.g.* [^{111}Ag]Ag^{+}) radiometals, forming highly stable complexes.[13–19] The N_2S_4 ligand series (**N_2S_4-Pa**, **N_2S_4-Py**, and **N_2S_4-Thio**) allows investigation of the effects of both the softness of pendant arm donor atoms and the macrocyclic ring size in comparison with our previously developed NS_4 ligand on [$^{197m/g}$Hg]Hg^{2+} radiolabeling and complex stability. With this work, we aim to expand the library of chelators for [$^{197m/g}$Hg]Hg^{2+} for future optimization and development of Hg-radiopharmaceuticals.

Herein, we describe the synthesis and characterization of the ligands, followed by the investigation of the Hg^{2+} coordination chemistry *via* nuclear magnetic resonance (NMR) spectroscopy accompanied by density functional theory (DFT) calculations to aid in elucidating the theoretical structure and bonding. [$^{197m/g}$Hg]Hg^{2+} radiolabeling studies were undertaken with radio-mercury produced on a medical cyclotron.[20] Subsequently, kinetic inertness of the resulting Hg-complexes was investigated through a series of *in vitro* assays against competitors such as human serum, glutathione (GSH) and biologically relevant metals ($ZnCl_2$, $FeCl_3$, $CuCl_2$, $MgCl_2$ and $CoCl_2$).

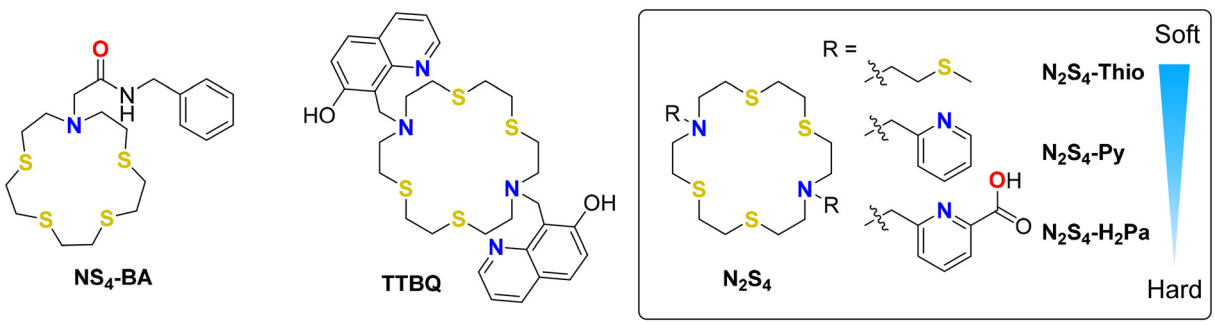

Fig. 1 The previously studied **NS_4-BA** (left), the mercury sensing **TTBQ** chelator (middle), and the novel N_2S_4 chelator series studied within bearing thioether (**N_2S_4-Thio**), pyridine (**N_2S_4-Py**), and picolinic acid (**N_2S_4-H_2Pa**) pendant arms, ranked based on their chemical "softness" (right).

Experimental

Materials and methods

All solvents and reagents were purchased from commercial suppliers and used as received unless otherwise noted. Ultrapure concentrated hydrochloric acid (HCl, 99.99% trace metal grade, 37%), sodium hydroxide (NaOH, 99.99% trace metal grade, pellets), ammonium acetate (NH_4OAc, 99.999% trace metal basis), dimethyl sulfoxide (DMSO), L-glutathione (GSH), metal salts ($ZnCl_2$, $FeCl_3$, $CuCl_2$, $MgCl_2$ and $CoCl_2$) and human serum were purchased from Sigma Aldrich (St Louis, MO). A Millipore system (Direct-Q® 3UV with Pump, 18 MΩ cm^{-1}) was used to obtain ultrapure water. Deuterated solvents used for NMR analysis were purchased from Sigma or Cambridge Isotope Laboratories Inc and exhibited an isotopic purity between 99.9% and 99.8%. Solvents noted as "dry" were obtained following storage over 3 Å molecular sieves under an argon atmosphere. All NMR spectra were recorded on a Bruker AVANCE III 600 MHz QCI cryoprobe, Bruker AVANCE III 500 MHz, or Bruker AVANCE III 400 MHz instruments. Chemical shifts are reported in parts per million (ppm) and are referred to as the residual solvent peak. Multiplicity is reported as follows: s = singlet, t = triplet, m = multiplet, and br = broad peak. The coupling constants (*J*) are reported in hertz (Hz). High-resolution electrospray-ionization mass spectrometry (ESI-HRMS) was performed on an Agilent 6210 time-of-flight instrument (TOF). Semi-preparative high performance liquid chromatography (HPLC) was performed using an Agilent Technologies 1100 system equipped with a quaternary pump, and a UV-vis detector monitoring at 254 nm, a Phenomenex Luna column (5 μm, C18, 100 Å, 150 × 10 mm), and a fraction collector were used for the analysis and semi-prep purification of **N_2S_4-Py**. Preparative HPLC was performed using an LC-20AP pump coupled to an SPD-20AV UV-vis detector monitoring at 270 nm (Shimadzu, Japan), and an ES Industries Epic Polar preparative column (10 μm, 120 Å, 25 cm × 20 mm) and a fraction collector were used for the analysis and semi-prep purification of **N2S4-Pa**. The radiolabeling of ligands was monitored using silica-impregnated instant thin-layer chromatography paper (iTLC-SG, Agilent Technologies, Santa Clara, CA, USA). Data were analyzed on an Eckert & Ziegler AR-2000 TLC scanner and processed using the Eckert & Ziegler WinScan software (Hopkinton, USA). A Capintec CRC-55tR dose calibrator well counter set at ^{197g}Hg calibration (calibration number: 197) was used to measure activity; Capintec activity readings were cross-referenced with the gamma spectrometer value to ensure accuracy in the reading values. The Capintec dose calibrator was used to measure the activity before radiolabeling reactions. A Bio-Rad Mini-PROTEAN Tetra Vertical Electrophoresis Cell instrument was used for all sodium dodecyl sulphate-polyacrylamide gel electrophoresis (SDS-PAGE) measurements with 4–20% Mini-PROTEAN® TGX™ Precast Protein Gels. The SDS-PAGE gel electrophoresis reagents, including the MW standards, TGS buffer, Laemmli sample buffer, and Bio-Safe™ Coomassie stain, were all purchased from Bio-Rad. All work with radionuclides at TRIUMF was undertaken in shielded fume hoods to minimize dose to experimenters (and special precautions were used to prevent contamination) under nuclear energy worker (NEW) status earned by attending TRIUMF's Advanced Radiation Protection course and passing the final exam.

Caution: $[^{197m/g}Hg]Hg^{2+}$ produces ionizing radiation and should be handled in laboratories approved and equipped for radioactive work using safe lab practices. Experiments should only be carried out by trained personnel.

Caution: Mercury is a toxic heavy metal, and its compounds should be treated accordingly.

Synthesis and characterization of N_2S_4 and derivatives

1,2-Ethanedithiol, chloroacetyl chloride, aminoethanethiol hydrochloride, dimethyl 2,6-pyridinedicarboxylate, 2-chloroethyl methyl sulfide and 2-(bromomethyl)pyridine hydrobromide were commercially obtained and used without further purification. Methyl 6-(chloromethyl)picolinate[21] and a solution of freshly prepared 1,10-diaza-4,7-dithiadecane[22] were synthesized following reported procedures. The N_2S_4 macrocycle synthesis was accomplished through modified procedures followed by Randhawa *et al.*[12]

***N*,*N*′-((Ethane-1,2-diylbis(sulfanediyl))bis(ethane-2,1-diyl)) bis(2-chloroacetamide) (1).** In a 100 mL flask under argon, K_2CO_3 (9.2 g, 67 mmol, 4 eq.) and the prepared 1,10-diaza-4,7-dithiadecane[22] (3.00 g, 16.6 mmol, 1 eq.) in 40 mL of dry dichloromethane were added. The flask was then cooled to 0 °C and stirred. Using an addition funnel, chloroacetyl chloride (~4 mL, 50 mmol, 3 eq.) diluted in 10 mL of dry dichloromethane was added to the reaction slowly over 30 min. During the course of 3 h at 0 °C, the formation of a substantial amount of white precipitate was observed. The reaction was then quenched by the addition of ice cold MilliQ water to the reaction until HCl gas evolution subsided. The solution was then filtered, and the precipitate was washed with cold dichloromethane, ether and MilliQ water and dried under vacuum to yield **1** as a white solid (3.35 g, 60%) which was used without any purification. ESI-HRMS *m*/*z* calcd for $[C_{10}H_{18}Cl_2N_2O_2S_2 + H]^+$ 333.027; found 333.002 $[M + H]^+$. ^{1}H NMR (400 MHz, $CDCl_3$) δ 7.08 (s, 2H), 4.09 (s, 4H), 3.54 (q, J = 6.5 Hz, 4H), 2.80 (s, 4H), 2.76 (t, J = 6.8 Hz, 4H). ^{13}C{^{1}H} NMR (101 MHz, $CDCl_3$) δ 166.09, 42.61, 39.10, 31.77, 31.41.

1,4,10,13-Tetrathia-7,16-diazacyclooctadecane-6,17-dione (2). Compound **2** was prepared from a suspension of **1** (3.33 g, 10.0 mmol, 1.00 eq.), 1,2-ethanedithiol (990 mg, 10.5 mmol, 1.05 eq.), and K_2CO_3 (5.54 g, 40.0 mmol, 4.00 eq.) in acetonitrile (600 mL). The solution was vigorously stirred under argon for 48 h at reflux. Once completion was verified by MS, the solvent was removed under vacuum. The residual solid was then washed with water, until the water layer was neutral, ensuring that all the excess K_2CO_3 was removed. The product was extracted from the precipitate using boiling chloroform (4 × 50 mL), and organic phases were collected and dried over Na_2SO_4. After filtration, the solvent was removed *in vacuo* to yield compound **2** as a white solid (1.80 g, 51% yield). ESI-HRMS *m*/*z* calcd for $[C_{12}H_{22}N_2O_2S_4 + NH_4]^+$ 372.091; found 372.101 $[M + NH_4]^+$. ^{1}H NMR (400 MHz, $CDCl_3$) δ 7.23 (s, 2H), 3.54 (q, J = 6.2 Hz, 4H), 3.28 (s, 4H), 2.90 (s, 4H), 2.86 (s, 4H),

2.79 (t, J = 6.5 Hz, 4H). $^{13}C\{^1H\}$ NMR (101 MHz, $CDCl_3$) δ 168.96, 38.91, 36.14, 32.92, 32.12, 31.81.

1,4,10,13-Tetrathia-7,16-diazacyclooctadecane (3). Compound **3** was synthesized following the modified literature procedure for similar macrocycles.[23] Under an argon atmosphere, excess borane tetrahydrofuran complex solution (1 M, ~30 mL, 30 mmol, 5.4 eq.) was added to a suspension of **2** (2.0 g, 5.64 mmol, 1 eq.) in dry THF (300 mL). The reaction was refluxed overnight under argon. After cooling the suspension to room temperature, the reaction was slowly quenched with water (15 mL) during which the solution turned homogeneous. Volatiles were removed under vacuum. The white solid obtained was suspended in 6 M HCl (20 mL) and refluxed for 3 h to obtain a homogeneous solution. The reaction mixture was cooled to 0 °C and basified (pH > 10) by slow addition of an aqueous solution of 10% NaOH (500 mL). The product was extracted using chloroform (3 × 30 mL), and organic phases were collected and dried over Na_2SO_4. After filtration, volatiles were removed under vacuum to yield a light-yellow oil which solidified upon standing. The crude product was purified by recrystallization from hot ether to yield **3** as a white solid (1.68 g, 91% yield). ESI-HRMS m/z calcd for $[C_{12}H_{26}N_2S_4 + H]^+$ 327.106; found 327.094 $[M + H]^+$. ^1H NMR (500 MHz, $CDCl_3$) δ 2.88 (t, J = 5.8 Hz, 8H), 2.82–2.76 (m, 16H), 1.78 (s, 2H). $^{13}C\{^1H\}$ NMR (101 MHz, $CDCl_3$) δ 48.07, 32.81, 32.48.

6,6′-((1,4,10,13-Tetrathia-7,16-diazacyclooctadecane-7,16-diyl)bis(methylene))dipicolinic acid H_2S_4macropa (N_2S_4-H_2Pa). The **N_2S_4-H_2Pa** macrocycle synthesis was accomplished through procedures followed by Randhawa *et al.*[12] To a solution of methyl 6-(chloromethyl)picolinate[24] (638 mg, 3.44 mmol, 2 eq.) and **3** (505 mg, 1.72 mmol, 1 eq.) in CH_3CN (50 mL) was added Na_2CO_3 (~1.1 g, 10.3 mmol, 6 eq.) and the reaction mixture was refluxed overnight. After cooling to room temperature, the reaction mixture was filtered, and the filtrate evaporated under vacuum to yield a light-yellow oil. The oil was redissolved in 4 M HCl (15 mL) and the reaction mixture was heated at 90 °C overnight. After cooling to room temperature, the volatiles were removed under vacuum at 60 °C. The light-yellow waxy residue thus obtained was purified by reverse-phase preparative high-performance liquid chromatography at 14 mL min^{-1} with the following method: A: H_2O with 0.1% TFA, B: MeOH with 0.1% TFA; 0–5 min 10% B, 5–25 min 10–100% B. Analytically pure fractions were combined, and volatiles were removed under vacuum. The residue was redissolved thrice in 4 M HCl (10 mL) and evaporated to dryness to remove residual TFA. The resulting white solid was redissolved in pure water (2 mL) and filtered and the filtrate was lyophilized to yield H_2S_4macropa (**N_2S_4-H_2Pa**) (680 mg, 53% yield). ESI-HRMS m/z calcd for $[C_{26}H_{36}N_4O_4S_4 + H]^+$ 597.170; found 597.128 $[M + H]^+$. ^1H NMR (500 MHz, D_2O) δ 7.89 (t, J = 7.7 Hz, 2H), 7.79 (d, J = 7.6 Hz, 2H), 7.59 (d, J = 7.6 Hz, 2H), 3.83 (s, 4H), 2.85–2.71 (m, 24H). $^{13}C\{^1H\}$ NMR (126 MHz, D_2O) δ 173.23, 157.27, 153.24, 138.38, 125.80, 122.42, 59.25, 53.15, 31.65, 28.28.

7,16-Bis(pyridin-2-ylmethyl)-1,4,10,13-tetrathia-7,16-diazacyclooctadecane (N_2S_4-Py). To a solution of 2-(bromomethyl) pyridine (386.98 mg, 1.53 mmol, 2.5 eq.) and **3** (200 mg, 0.612 mmol, 1 eq.) in CH_3CN (10 mL), K_2CO_3 (338.6 mg, 2.45 mmol, 4 eq.) and KI (10.13 mg, 0.061 mmol, 0.1 eq.) were added. The reaction mixture was heated at 60 °C overnight under argon. After cooling to room temperature, the mixture was evaporated under vacuum, then washed with water and brine (2 × 5 mL each) and extracted using dichloromethane (3 × 30 mL). Organic phases were collected and dried over Na_2SO_4. After filtration, volatiles were removed under vacuum to yield a light-yellow oil. The recovered oil was further purified by reverse-phase semipreparative high-performance liquid chromatography at 4.5 mL min^{-1} with the following method: A: H_2O with 0.1% TFA, B: acetonitrile (CH_3CN) with 0.1% TFA; 0–0.5 min 0% B; 0.5–10 min 0–100% B, 10–11 min 100% B. The fraction at 6.04 min was collected and lyophilized to yield **N_2S_4-Py** (70 mg, 23% yield) as a yellow solid. ESI-HRMS m/z calcd for $[C_{24}H_{36}N_4S_4 + H]^+$ 509.190; found 509.195 $[M + H]^+$. ^1H NMR (600 MHz, CD_3CN) δ 8.64 (d, J = 4.3 Hz, 2H), 7.89 (td, J = 7.7, 1.8 Hz, 2H), 7.49 (d, J = 7.8 Hz, 2H), 7.46 (dd, J = 7.7, 5.0 Hz, 2H), 4.43 (s, 4H), 3.47 (t, 8H), 2.98 (t, 8H), 2.81 (s, 8H). $^{13}C\{^1H\}$ NMR (151 MHz, CD_3CN) δ 159.82, 148.82, 136.35, 122.98, 122.03, 60.13, 54.03, 32.15, 29.57.

7,16-Bis(2-(methylthio)ethyl)-1,4,10,13-tetrathia-7,16-diazacyclooctadecane (N_2S_4-Thio). To a stirring solution of 2-chloroethyl methyl sulfide (84.6 mg, 0.765 mmol, 2.5 eq.) and **3** (100 mg, 0.306 mmol, 1.0 eq.) in CH_3CN (5 mL), K_2CO_3 (169.27 mg, 1.22 mmol, 4.0 eq.) and KI (5.08 mg, 0.031 mmol, 0.1 eq.) were added. The reaction mixture was heated to 60 °C overnight under argon. After cooling to room temperature, the mixture was evaporated under vacuum, then washed with water and brine (2 × 5 mL each) and extracted using dichloromethane (3 × 30 mL). Organic phases were collected and dried over Na_2SO_4. After filtration, volatiles were removed under vacuum to yield a light-yellow oil. Flash chromatography of the resulting residue (silica; dichloromethane–EtOAc 9 : 1, R_f = 0.09) gave **N_2S_4-Thio** (66 mg, 45% yield) as a white crystalline solid. ESI-HRMS m/z calcd for $[C_{18}H_{38}N_2S_6 + H]^+$ 475.144; found 475.161 $[M + H]^+$. ^1H NMR (600 MHz, $CDCl_3$) δ 2.81 (s, 8H), 2.78–2.73 (m, 12H), 2.70–2.67 (m, 8H), 2.62–2.58 (m, 4H), 2.13 (s, 6H). $^{13}C\{^1H\}$ NMR (151 MHz, $CDCl_3$) δ 54.37, 54.17, 32.76, 31.97, 30.62, 15.94.

Preparation of non-radioactive $^{nat}Hg^{2+}$ complexes for NMR studies

The $^{nat}Hg^{2+}$ complexes for NMR characterization were prepared *via* the addition of 50 μL of a ligand solution (10^{-2} M, in DMSO-d_6) and 5 μL of $HgCl_2$ (10^{-1} M, in DMSO-d_6), resulting in an equimolar metal-to-ligand ratio. The solutions were then diluted up to 450 μL in DMSO-d_6 for NMR studies. Complex formation was confirmed by ESI-HRMS. These complexes were used in variable temperature and time dependent complex-formation experiments where the NMR of the solution was performed at 1 h, 6 h and 24 h post addition of the metal to the ligand solution. All data were collected using the standard Bruker parameters and processed using the MestReNova 14.1.2-25024 software.

[^{nat}Hg(N_2S_4-Pa)]. ESI-HRMS *m*/*z* calcd for $[C_{26}H_{34}N_4O_4S_4Hg + H]^+$ 797.125; found 797.166 $[M + H]^+$. ^{1}H NMR (600 MHz, DMSO-d_6) δ 8.12 (dt, J = 14.3, 7.6 Hz, 4H), 7.79 (d, J = 7.4 Hz, 2H), 4.65 (s, 4H), 3.03 (s, 8H), 2.83 (s, 8H). [8H are missing from the integration as this proton peak is under the DMSO-d_6 solvent signal; this has been confirmed by the ^{1}H–^{1}H homonuclear correlation spectroscopy (COSY) and ^{1}H–^{13}C heteronuclear single quantum coherence (HSQC) data]. ^{13}C{^{1}H} NMR (151 MHz, DMSO-d_6) δ 139.69, 125.13, 128.04, 55.88, 54.26, 47.31, 24.47 (assigned by HSQC, 4 quaternary carbons missing, 2 aromatic and 2 carbonyl).

[^{nat}Hg][Hg(N_2S_4-Py)]$^{2+}$. ESI-HRMS *m*/*z* calcd for $[(C_{24}H_{36}N_4S_4Hg)^{2+} + Cl^-]^+$ 745.121; found 745.111 $[M + Cl]^+$. ^{1}H NMR (600 MHz, DMSO-d_6) δ 8.66 (d, 2H), 8.51–8.47 (m, 1H), 8.01 (s, 1H), 7.78 (s, 1H), 7.60 (d, J = 7.9 Hz, 1H), 7.43 (t, J = 7.2 Hz, 1H), 7.29 (s, 1H), 3.85 (s, 4H), 3.10–2.69 (m, 24H). ^{13}C{^{1}H} NMR (151 MHz, DMSO-d_6) δ 148.56, 139.50, 137.89, 137.24, 128.18, 124.94, 123.33, 122.03, 49.87, 45.99, 36.93, 36.61, 35.64, 33.37, 30.78, 30.46, 29.17, 28.19, 27.55, 26.25, 24.31 (assigned by HSQC, 2 quaternary aromatic carbons missing).

[^{nat}Hg][Hg(N_2S_4-Thio)]$^{2+}$. ESI-HRMS *m*/*z* calcd for $[(C_{18}H_{38}N_2S_6Hg)^{2+} + Cl^-]^+$ 711.075; found 711.078 $[M + Cl]^+$. ^{1}H NMR (600 MHz, DMSO-d_6) δ 3.03–2.57 (m, 32H), 2.10 (s, 6H). ^{13}C{^{1}H} NMR (151 MHz, DMSO-d_6) δ 52.97, 33.88, 31.94, 30.97, 30.00, 29.67, 27.41, 15.44 (assigned by HSQC).

DFT calculations

DFT calculations were performed using the Gaussian 16 software for all geometry optimizations, frequency analysis, and thermodynamic data that were extracted.[25] Calculations were performed with the Becke three parameter, Lee–Yang–Parr (B3LYP) functional with the triple-ζ 6-311G** basis set for all the main group elements in the novel sulfur backbone derivatives (H, C, N, O, S) and were corrected with Grimme's dispersion correction along with Becke–Johnson damping (D3-BJ).[26–29] The Stuttgart Dresden (SDD) small-core effective core potential (ECP) along with the respective SDD basis set was used for Hg to include scalar relativistic effects.[30] Structures were optimized in water using the polarizable continuum model (PCM).[31] All conformers were created by constructing all possible stereochemically unique backbone/sidearm combinations manually and optimizing them at the molecular mechanics (MM) level of theory using the universal force field (UFF) and the default parameters in the Avogadro software.[32] Structures were then re-optimized using the B3LYP level of theory with hybrid basis sets (6-311G**/SDD) until all possible chemically reasonable structures were obtained. Vibrational frequency calculations were performed at the optimized geometries to ensure that minima were obtained and to obtain solvated thermochemistry data. The Gibbs free energy of solvation was used to estimate the aqueous stability of each conformer in solution using the gas phase Gibbs energy and the Gibbs energy of solvation (eqn (1)):[33]

$$G_{soln} = G_{gas} + \Delta G_{solv} \quad (1)$$

These energies were calculated with the zero-point energy correction and scaled by 0.967, the corresponding scaling factor for B3LYP-6-311G** calculations.[34] More details on the calculations of these values are given in ESI Tables S1–3.† Geometry optimizations were performed without imposing any symmetric constraints. Structures were visualized using the Mercury software package.[10]

Production of mercury-197m/g

The production of $[^{197m/g}Hg]Hg^{2+}$ was achieved through proton irradiation of natural gold (Au) targets *via* the ^{197}Au(p, n)$^{197m/g}$Hg nuclear reaction at the TR13 (13 MeV) cyclotron at TRIUMF – Canada's particle accelerator center, following previously published procedures, with calculated rates of production of 4 MBq μA^{-1} h^{-1} for ^{197m}Hg and 2.9 MBq μA^{-1} h^{-1} for ^{197g}Hg.[20] Briefly, Au targets were prepared by the addition of 200–270 mg of Au foil to a 10 mm diameter indent (0.25 mm deep) of a tantalum backing (1 mm in thickness) and melted thereon in a furnace at 1250 °C (Rd-G – RD Webb Company – Natick MA, USA). Following proton irradiation (4 h, 30 μA, 13 MeV), the Au target was dissolved in *aqua regia* (3 mL), and the solution was then loaded onto a prepared column of LN resin (5 g, 25 mL reservoir). $^{197m/g}Hg^{2+}$ was eluted in 6 M HCl (4 mL) while the ^{197}Au was retained on the resin. The $^{197m/g}Hg^{2+}$ solution matrix was then exchanged to a 0.1 M HCl solution by multiple steps of evaporation and reconstitution. The final activity ranged from 90 to 140 MBq of $^{197m/g}Hg^{2+}$ obtained as $HgCl_2$ in 250–350 μL of 0.1 M HCl. The radionuclide purity was evaluated using gamma (γ)-ray spectroscopy on an N-type co-axial high-purity germanium (HPGe) gamma spectrometer (CANBERRA, Mirion Technologies, Inc., San Ramon, CA, USA), calibrated with a 20 mL ^{152}Eu and ^{133}Ba source. Samples were prepared by mixing aliquots of $^{197m/g}Hg^{2+}$ activity (1.2 MBq) with deionized water in a 20 mL glass vial to make a 20 mL sample and measured at a distance of 150 mm from the detector for 10 min, ensuring that dead times were below 10%. Spectra were analyzed using the Genie-2000 software, using the 133.98 keV (I_γ = 33.5%) and 164.97 keV (I_γ = 0.2618%) γ-lines of ^{197m}Hg, and the 77.35 keV (I_γ = 18.7%) γ-line of ^{197g}Hg for activity calculations. The radionuclidic purity was >99%.[20]

[$^{197m/g}$Hg]Hg^{2+} radiolabeling studies. The ligands **N_2S_4-Py**, **N_2S_4-H_2Pa** and **N_2S_4-Thio** were made up as stock solutions (10^{-3} M) in deionized water or a DMSO–water mixture. A serial dilution was used to prepare ligand solutions at 10^{-4}, 10^{-5} M, 10^{-6} M, and 10^{-7} M in water. An aliquot (10 μL) of each ligand solution (or water, for negative controls) was diluted with ammonium acetate buffer (1 M; pH 7) such that the final reaction volume was 100 μL after the addition of activity. [$^{197m/g}$Hg]$HgCl_2$ (1–1.2 MBq, 3–10 μL) was mixed gently to begin the radiolabeling reaction at 80 °C or room temperature. Complex formation was monitored for each reaction by acquiring the non-isolated percentage radiochemical yield (%RCY) at 1 h. This was achieved firstly by extracting an aliquot (10 μL) of the reaction solution and quenching it with an equal volume of dimercaptosuccinic acid (DMSA) solution (50 mM, pH 5, 10 μL). The

quenched solution was gently mixed and analyzed by spotting a portion (10 μL) of the mixture onto the bottom of an iTLC-SG plate (1 cm × 10 cm, baseline at 1 cm) and then developed using DMSA solution (50 mM, pH 5) as the mobile phase. Under these conditions, the [^{197m}Hg]Hg^{2+}-complexes remain at the baseline (R_f = 0), while the unchelated, 'free' $^{197m/g}$Hg^{2+} migrates towards the solvent front (R_f = 1). TLC plates were analyzed on an Eckert & Ziegler AR-2000 TLC scanner and processed using the Eckert & Ziegler WinScan software. Radiolabeling yields were calculated by integrating the peaks in the radio-chromatogram. **Note*: Although ammonium acetate is not an ideal buffer at pH 7, it is commonly used for radiolabeling reactions. In our previous work,[10] we found that a 1 M ammonium acetate buffer at pH 7 was the most effective for $^{197m/g}$Hg radiolabeling reactions, outperforming other pH 7 buffers such as HEPES and PBS.

Stable metal competition assay

To solutions of [$^{197m/g}$Hg]**[Hg(N$_2$S$_4$-Py)]$^{2+}$**, [$^{197m/g}$Hg]**[Hg(N$_2$S$_4$-Pa)]**, or [$^{197m/g}$Hg][Hg(**N$_2$S$_4$-Thio**)]$^{2+}$ (prepared as described above) or radiolabeling controls (deionized water instead of the ligand) was added 10 μL of a 10 mM metal solution of biologically relevant metals ($ZnCl_2$, $FeCl_3$, $CuCl_2$, $MgCl_2$ and $CoCl_2$) in water. The final solution contained a 10-fold excess of the stable metal to the chelators and a 10^6-fold excess of the stable metal to $^{197m/g}$Hg^{2+} in solution. The mixtures were incubated at room temperature (RT) over 82 h. The proportion of the intact radiolabeled complex was monitored over the course of 82 h using iTLC-SG and DMSA solution (50 mM, pH 5) as the mobile phase. Under these conditions, uncomplexed $^{197m/g}$Hg^{2+} resulting from stable metal transchelation traveled to the solvent front (R_f = 1) while intact [$^{197m/g}$Hg]**[Hg(N$_2$S$_4$-Py)]$^{2+}$**, [$^{197m/g}$Hg]**[Hg(N$_2$S$_4$-Pa)]** or [$^{197m/g}$Hg]**[Hg(N$_2$S$_4$-Thio)]$^{2+}$** remained at the baseline (R_f = 0).

Glutathione (GSH) competition assay

GSH competition assay procedures closely followed those previously developed by our group.[10] [$^{197m/g}$Hg]**[Hg(N$_2$S$_4$-Py)]$^{2+}$**, [$^{197m/g}$Hg]**[Hg(N$_2$S$_4$-Pa)]**, and [$^{197m/g}$Hg]**[Hg(N$_2$S$_4$-Thio)]$^{2+}$** (prepared as described above) or radiolabeling controls (deionized water instead of the ligand) were added to a 50 mM L-glutathione (GSH) solution (1 : 22 v/v GSH : reaction solution dilution), and the mixtures were incubated at 37 °C over 24 h. The final GSH concentration was chosen to mimic *in vivo* conditions within cells (2.12 mM).[35] The proportion of the intact radiolabeled complex was monitored over the course of 24 h using iTLC-SG and L-glutathione (50 mM) as the mobile phase. Under these conditions, uncomplexed $^{197m/g}$Hg^{2+} resulting from GSH transchelation traveled to the solvent front (R_f = 1) while intact [$^{197m/g}$Hg]**[Hg(N$_2$S$_4$-Py)]$^{2+}$**, [$^{197m/g}$Hg]**[Hg(N$_2$S$_4$-Pa)]**, or [$^{197m/g}$Hg]**[Hg(N$_2$S$_4$-Thio)]$^{2+}$** remained at the baseline (R_f = 0).

Human serum stability assay

[$^{197m/g}$Hg]**[Hg(N$_2$S$_4$-Py)]$^{2+}$**, [$^{197m/g}$Hg]**[Hg(N$_2$S$_4$-Pa)]**, and [$^{197m/g}$Hg]**[Hg(N$_2$S$_4$-Thio)]$^{2+}$** (prepared as described above) or radiolabeling controls (deionized water instead of the ligand) were diluted in human serum (1 : 1 v/v dilution), and the solutions were incubated at 37 °C over 72 h. The metal-complex stabilities were monitored over 72 h using SDS-PAGE. At each time point, an aliquot (10 μL) of the reaction mixture was mixed with Laemmli sample buffer (10 μL) and was directly loaded onto the SDS-PAGE gel. The SDS-PAGE was run at ambient temperature and 150 V until the dye front reached the resolving gel (1 h). Following electrophoresis, the gel was scanned with the radio-TLC scanner to determine the percentage of the intact complex. The same protocol was used with 'free' [$^{197m/g}$Hg]Hg^{2+} and each of the $^{197m/g}$Hg^{2+}-complexes diluted in phosphate-buffered saline (PBS) (5 μL;1 : 1 v/v dilution) to assess their electrophoretic mobility.

Results and discussion

Synthesis and characterization of the N$_2$S$_4$ ligand series

The N_2S_4 macrocyclic backbone was synthesized using modified procedures adapted from our previous work (Scheme 1).[12] First, 1,2-bis(2-aminoethylthio)ethane was synthesized *via* the addition of aminoethanethiol hydrochloride to dibromoethane under inert and basic conditions following procedures by Khanmohammadi *et al.*[22] The product was then kept under an inert atmosphere until ready for use, to limit its reaction with carbon dioxide in the atmosphere. Subsequently, chloroacetyl chloride was added to 1,2-bis(2-aminoethylthio)ethane under basic conditions, producing **1**. Without purification, cyclization of **1** was carried out immediately after isolation to avoid degradation of the acyl chlorides, with 1,2-ethanediothiol yielding **2** in 51% yield. The carbonyls on macrocycle **2** were reduced utilizing BH_3-THF, yielding the N_2S_4 backbone (**3**) in

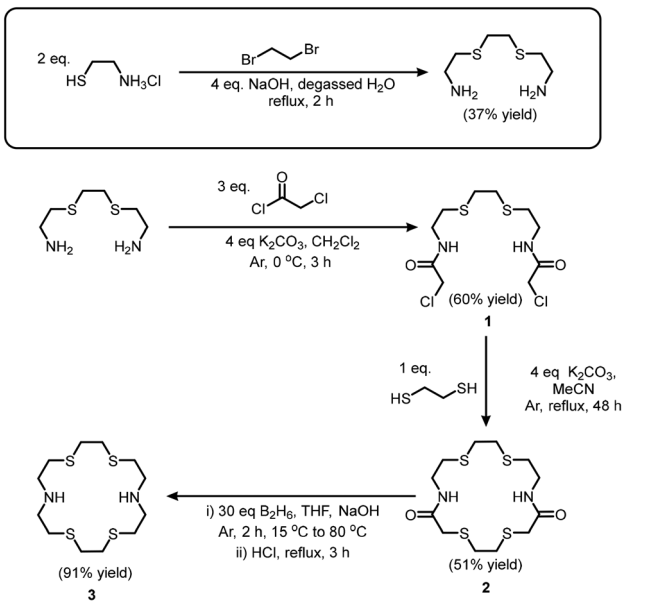

Scheme 1 Synthetic procedures for the N_2S_4 macrocyclic backbone.

91% yield. Following the synthesis of the backbone, alkylation of the secondary amines (with methyl 6-(chloromethyl)picolinate, 2-(bromomethyl)pyridine or 2-chloroethyl methyl sulfide) was undertaken (**N_2S_4-H_2Pa** required an additional deprotection step of the methyl esters) following previously reported procedures yielding **N_2S_4-H_2Pa**, **N_2S_4-Py** and **N_2S_4-Thio** (Scheme 2). All ligands and intermediates were characterized by NMR and MS (reported in Fig. S1–S12†). Overall, starting from the N_2S_4 macrocycle (**3**), the three chelators were prepared in yields between 23–53%; the relatively low chemical yields could be attributed to losses during HPLC purification of the final chelators.

Synthesis and characterization of non-radioactive Hg^{2+} complexes

To investigate the solution coordination chemistry and binding efficiency of the N_2S_4 ligand series with Hg^{2+}, the metal complexes were prepared by the addition of the ligand and metal in a deuterated DMSO solution to form a 1 : 1 equivalent metal-to-ligand complex. All complexes were then characterized *via* NMR spectroscopy (reported in Fig. 2 and S13–S23†) and high-resolution mass spectrometry (HRMS) (Fig. S24–26†). ^{1}H NMR acquisitions were performed at several time points (1, 6 and 24 h at 25 °C) after solution preparation to observe time-dependent complex formation (Fig. S14, S17 and S21†). MS and NMR confirmed all complexes formed within an hour upon addition of the metal to the ligand. MS spectra demonstrated a 1 : 1 metal–ligand complex with the corresponding unique Hg isotope distribution pattern (Fig. S24–26†). Upon complexation, downfield shifting in the macrocyclic backbone resonances of **$[Hg(N_2S_4$-Py$)]^{2+}$** (δ 2.72 → 2.91 ppm) and **$[Hg(N_2S_4$-Thio$)]^{2+}$** (δ 2.68 → 2.74 ppm) were observed. Downfield shifting in the pendant arm methylene proton resonances of **$[Hg(N_2S_4$-Py$)]^{2+}$** (δ 3.79 → 3.85 ppm) and the CH_3 singlet of the thioether in **$[Hg(N_2S_4$-Thio$)]^{2+}$** (δ 2.06 → 2.10 ppm) at 25 °C can also be observed. The downfield shifting of proton resonances close to donor atoms, which interact with the metal center, is indicative of metal–ligand binding due to the electron-withdrawing effects of the electron-deficient metal. Furthermore, the proton resonances associated with the macrocyclic backbone (δ ~2.5–3.2 ppm) for both **$[Hg(N_2S_4$-Thio$)]^{2+}$** and **$[Hg(N_2S_4$-Py$)]^{2+}$** resulted in peak broadening indicative of a fluxional complex occurring on the NMR timescale and/or the existence of different isomers in solution. The NMR spectra of **$[Hg(N_2S_4$-Py$)]^{2+}$** and **$[Hg(N_2S_4$-Thio$)]^{2+}$** were also investigated at 45 °C (Fig. S18 and S22,† respectively) in which coalescence of the macrocyclic backbone proton resonances was observed upon increasing the temperature to 45 °C, further suggesting the presence of a fluxional species in solution at ambient temperature. However, some spectral broadness was still observed and is likely attributed to the loss of symmetry of the **N_2S_4-Py** and **N_2S_4-Thio** chelators upon metal complexation.

Characterization of the carbon peaks assigned by HSQC (^{13}C NMR signals too weak for assignment) provides evidence of the formation of an asymmetric complex. The **$[Hg(N_2S_4$-Py$)]^{2+}$** HSQC spectrum at 25 °C displayed 21 carbon peaks; 8 aromatic and 13 aliphatic carbon peaks, suggesting that all the carbons, except the pendant arm CH_2 carbons, are in non-equivalent chemical environments upon complexation. The

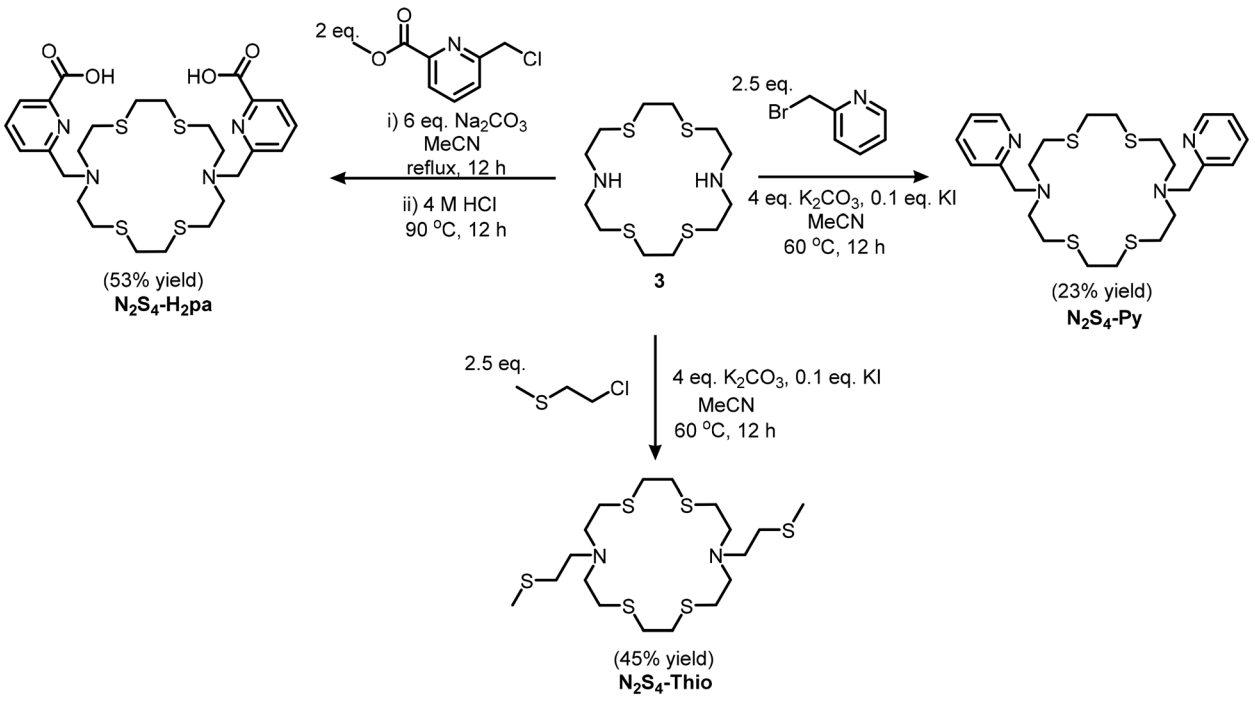

Scheme 2 Synthetic procedures of the N_2S_4 derivatives **N_2S_4-H_2Pa**, **N_2S_4-Py** and **N_2S_4-Thio**.

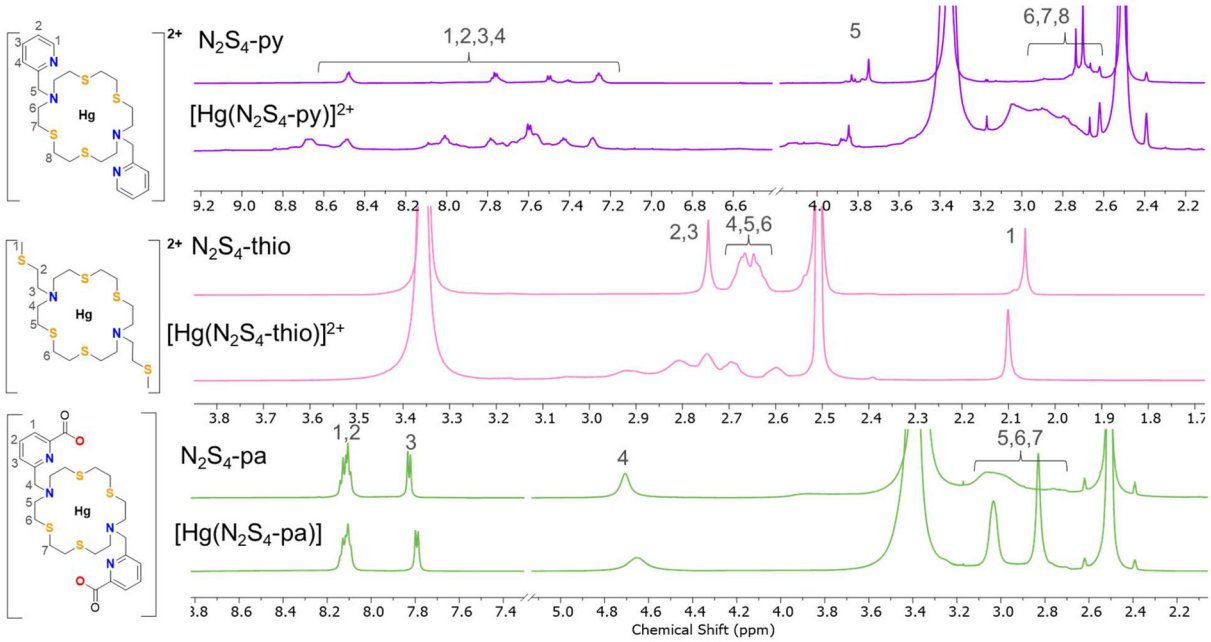

Fig. 2 ^{1}H NMR spectra of **N_2S_4-Py**, **N_2S_4-Thio** and **N_2S_4-H_2Pa**, and their $^{nat}Hg^{2+}$ complexes (600 MHz, DMSO-d_6, 25 °C).

HSQC spectrum of **[Hg(N_2S_4-Thio)]$^{2+}$** at 25 °C also suggests an increase in asymmetry upon complexation, agreeing with the DFT structure proposed below; of the 12 carbons within the macrocyclic backbone, 5 unique carbon resonances are present upon complexation, compared to the symmetric ligand for which 3 different chemical environments were observed. An additional 3 signals were assigned to the thioether pendant arms.

In contrast, the formation of the **[Hg(N_2S_4-Pa)]** complex demonstrated enhanced rigidity with respect to the free ligand as the backbone proton resonances alter from a broad singlet to two more defined singlets upon complexation (Fig. 2). Symmetry can be observed in the complex as the HSQC NMR exhibited 7 carbon signals: 3 aromatic, 1 pendant methylene, and 3 macrocycle peaks, indicating that the chemical equivalence of the carbons on the ligand is preserved upon metal complexation.

Challenge assays between the ^{nat}Hg-complexes and the soft-donor ligand DMSA (dimercapto succinic acid) were also attempted to assess dissociation kinetics of the Hg-complexes; however, due to overlapping of proton resonances in the N_2S_4 chelators and DMSA, the NMR spectra were difficult to elucidate, and no conclusions could be drawn. Instead, competition assays at the radiotracer scale using [$^{197m/g}$Hg]Hg-labeled chelators were conducted to discern the inertness of the complexes (see below).

Density functional theory calculations

Density functional theory (DFT) calculations were performed to aid in elucidating the aqueous solution structure of the three Hg^{2+}-N_2S_4 complexes. All possible conformers were generated and optimized, producing the Gibbs energies in the gas (ΔG_{gas}) and solution (ΔG_{soln}) phases (Tables S1–S3†). Each conformer is assigned their configuration by first *cis* or *trans*, orientating the pendant arm relative to each other, where *cis* indicates the two pendant arms are on the same face of the complex, resulting in a facial complex. In comparison, *trans* indicates the two arms are situated on opposite sides of the complex, resulting in a meridional complex. Delta (δ) and lambda (λ) assignments refer to the "twist" of the ethylene groups in the macrocycle's 6-membered chelate rings upon metal complexation (δ/λ; clockwise/counterclockwise). The X-ray crystal structure of the Hg^{2+} complex with the N_2S_4 backbone without any pendant arms ([Hg(N_2S_4)]$^{2+}$) has been reported in the literature to form a 6-coordinate complex with all the N_2S_4 donor atoms of the macrocycle.[36]

The thermodynamically stable gas-phase (ΔG_{gas}) **[Hg(N_2S_4-Py)]$^{2+}$** structure is a 6-coordinate complex (configuration 5; Fig. 3) in a *cis* (δ,λ,δ,λ,λ,λ) configuration (Table S1†) where the four sulfur atoms of the N_2S_4 macrocycle form a triangular prism with the two pyridines capping either side of the vertex (N_2S_4 coordination), satisfying the coordination sphere of the Hg^{2+} cation. The backbone amines weakly interact outside the sphere at distances of 3.000 and 2.985 Å. This structure provides optimal orientation of the thioether backbone groups, enabling access to the bulky pyridine pendant arms while limiting steric and electrostatic repulsion.[37] However, conformer 9 (Fig. 3) becomes the true energy minimum when the solvation effects are considered (ΔG_{soln}). This structure adopts a 6-coordinate *cis* (λ,λ,δ,δ,λ,δ) distorted octahedral arrangement, with 3 of the backbone sulfurs (d_{S1-Hg} = 2.724 Å, d_{S2-Hg} = 2.925 Å, d_{S3-Hg} = 2.773 Å), the two pyridines (d_{N3-Hg} = 2.435 Å, d_{N4-Hg} = 2.539 Å), and one of the backbone amines (d_{N4-Hg} = 2.693 Å), all strongly interacting in the coordination sphere of Hg^{2+},

given by the covalent radii of N and S of 0.71 Å and 1.05 Å, respectively.[38] The next nearest low energy structure (Table S1,† conformer 6) is 4.7 kJ mol^{-1} higher in energy than conformer 9. Gibbs energy differences up to 5 kJ mol^{-1} can be present in solution,[39] suggesting that conformer 9 will be the main configuration in solution; however, conformer 6 may be present in solution as a minor product. Conformer 9 exhibits C_1 symmetry, agreeing with the designation observed in the NMR spectra of **[Hg(N$_2$S$_4$-Py)]$^{2+}$** (*vide supra*, Fig. 2). The difference in the lowest energy conformation between the gas (conformer 5) and solution phases (conformer 9) is likely due to the macrocyclic ligand solvation effect[40] and the hydrophobic effect.[41] The hydrophobic effect results in the aggregation of hydrophobic particles to minimize entropic destabilization of water molecules.[42] Thus, the tighter arrangement of the pyridine pendant arms in the solution phase structure (conformer 9, bond angle of $N_{pyridine}$–Hg–$N_{pyridine}$: 76.05°), relative to the gas phase structure (conformer 5, bond angle of $N_{pyridine}$–Hg–$N_{pyridine}$: 78.12°), results in the tighter orientation of the backbone in the solution phase (conformer 9) which minimizes interactions between the polar water and the non-polar macrocyclic backbone (Fig. 3).

The lowest energy gas phase configuration of **[Hg(N$_2$S$_4$-Thio)]$^{2+}$** (conformer 11; ΔG_{gas} = 0.0 kJ mol^{-1}) adopts a 6-coordinate distorted octahedral complex with the backbone in a *cis* (λ,δ,δ,δ,λ,δ) orientation (Table S3† and Fig. 4), wherein the mercury cation is strongly coordinated by all four backbone sulfurs and both thioether arms (S_6 coordination) with an average Hg–S interatomic distance of 2.835 Å ($d_{S1–Hg}$ = 2.939 Å, $d_{S2–Hg}$ = 2.857 Å, $d_{S3–Hg}$ = 2.861 Å, and $d_{S4–Hg}$ = 2.696 Å, $d_{S5–Hg}$ = 2.961 Å, $d_{S6–Hg}$ = 2.698 Å; Table S4†). This structure adopts the most diffuse orientation for all the sulfur heteroatoms, maximizing the interatomic S–S distances to accommodate sulfur's relatively large covalent radius while minimizing the S–Hg bond distances. However, as was seen in the case of **[Hg(N$_2$S$_4$-Py)]$^{2+}$**, solvation effects play a role in the metal-complex geometry in solution. The calculated lowest energy conformation of **[Hg(N$_2$S$_4$-Thio)]$^{2+}$** in solution becomes conformer 7 with the backbone in a *cis* (δ,λ,δ,λ,δ,λ) arrangement. The complex adopts a five-coordinate distorted trigonal pyramidal arrangement with three backbone sulfurs and both pendant arm sulfurs coordinated (S_5 coordination). This configuration forms a tight binding pocket with both pendant arms on the same face with an average Hg–S bond distance of 2.788 Å ($d_{S1–Hg}$ = 2.941 Å, $d_{S2–Hg}$ = 2.767 Å, $d_{S3–Hg}$ = 2.596 Å, $d_{S5–Hg}$ = 2.658 Å, $d_{S6–Hg}$ = 2.787 Å; Table S5†), resulting in a hydrophobic compartment[42] shielding and excluding solvent from the complex cavity, increasing the stability as a result of the hydrophobic effect. Conformer 7 can also be defined as having a C_1 symmetry, which agrees with the **[Hg(N$_2$S$_4$-Thio)]$^{2+}$** NMR spectral observations (*vide supra*, Fig. 2).

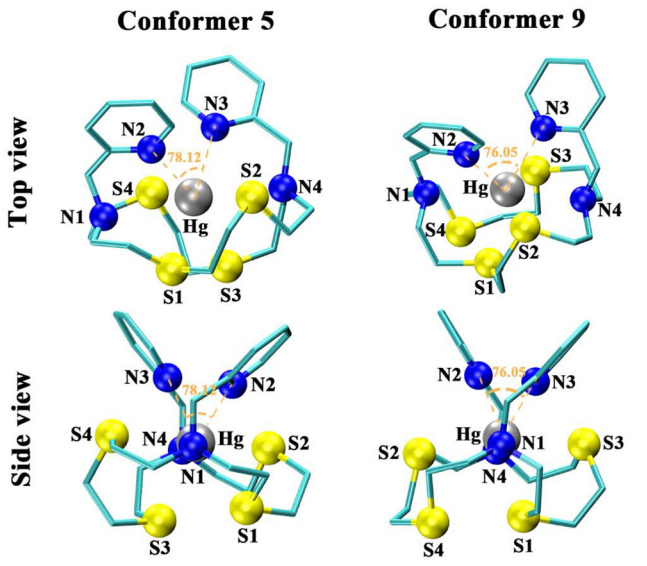

Fig. 3 Lowest-energy B3LYP-6-311G**/SDD optimized geometry of the **Hg-N$_2$S$_4$-Py** complex in the gas phase (conformer 5) and in solution (conformer 9). Hydrogen atoms were omitted for clarity. The $N_{pyridine}$–Hg–$N_{pyridine}$ angles ($N_{pyridine}$ = N2 and N3) are indicated in orange.

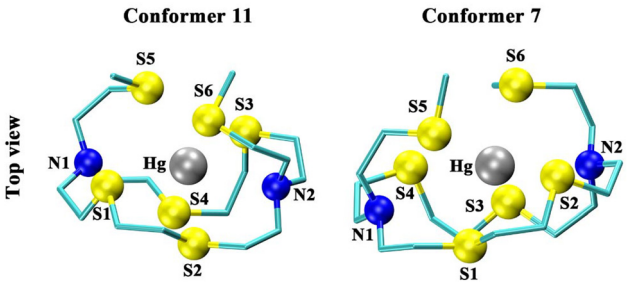

Fig. 4 Lowest energy B3LYP-6-311G**/SDD optimized geometry of the **N$_2$S$_4$-Thio** Hg-complex in the gas phase (conformer 11) and solution phase (conformer 7). Hydrogen atoms were omitted for clarity.

Within the **[Hg(N$_2$S$_4$-Pa)]** structures, a universal energy minimum (ΔG_{soln}, ΔG_{gas} = 0.0 kJ mol^{-1}) conformer exists, and conformer 7 (*cis* (δ,δ,λ,δ,δ,δ)) demonstrates strong coordination with the picolinic acid heteroatoms ($d_{O1–Hg}$ = 2.471 Å, $d_{O2–Hg}$ = 2.380 Å, $d_{N2–Hg}$ = 2.524 Å, $d_{N3–Hg}$ = 2.450 Å) and one of the backbone sulfur atoms ($d_{S1–Hg}$ = 2.659 Å), while weak interactions are observed with another sulfur donor ($d_{S2–Hg}$ = 3.480 Å). Along with conformer 7, the solution phase structure optimization of **[Hg(N$_2$S$_4$-Pa)]** gave two other unique low energy structures, conformers 9 and 3 (Table S5†) with relative Gibbs energy in solution of 1.6 kJ mol^{-1} and 3.6 kJ mol^{-1}, respectively. The energy differences are small enough that all conformers could be present in solution. Conformer 9 (*cis* (λ,λ,δ,δ,δ,λ)) (ΔG_{gas} = 0.6 kJ mol^{-1}, ΔG_{soln} = 1.6 kJ mol^{-1}), demonstrates Hg^{2+} strongly interacting with the picolinic acid pendant arms ($d_{O1–Hg}$ = 2.445 Å, $d_{O2–Hg}$ = 2.431 Å, $d_{N2–Hg}$ = 2.482 Å, $d_{N3–Hg}$ = 2.442 Å), and two sulfur atoms ($d_{S1–Hg}$ = 2.756 Å, $d_{S4–Hg}$ = 2.731 Å), differing from the coordination of conformer 7. Conformer 3 (*cis* (λ,δ,δ,δ,λ,δ)) has a Gibbs energy in solution of 3.6 kJ mol^{-1} and adopts the same binding motif as conformer 7 ($d_{O1–Hg}$ = 2.378 Å, $d_{O2–Hg}$ = 2.413 Å, $d_{N2–Hg}$ = 2.444 Å, $d_{N3–Hg}$ = 2.417 Å, $d_{S1–Hg}$ = 2.737 Å, $d_{S4–Hg}$ = 3.095 Å),

but differs in that the two picolinic acids are flush with the metal–ligand plane instead of perpendicular. Conformer 3 is the only conformer with significantly higher gas phase Gibbs energy (ΔG_{gas} = 33.6 kJ mol^{-1}) compared to the solution phase (ΔG_{soln} = 3.6 kJ mol^{-1}), suggesting that the structure benefits the most energetically from solvation. As the picolinic acids are flush with the backbone, a binding pocket is created, increasing the stability due to the hydrophobic effect. The three lowest energy structures are all stereochemically unique; however, they form the same arrangement in space with slight changes in the overall conformation of the sulfurs in the backbone, as conformers 7 and 9 interact with two opposing sulfur atoms, while conformer 3 interacts with two sulfur atoms adjacent to the nitrogen. All three strongly interact with the 4 picolinic acid chelating heteroatoms (carboxyl oxygen and pyridine nitrogens), resulting in a rectangular plane that is symmetrically capped by two of the sulfurs in the backbone that are flush with this plane (Fig. 5). The presence of the three conformers in solution is consistent with the **[Hg(N_2S_4-Pa)]** NMR (*vide supra*, Fig. 2), producing two backbone resonances with low resolutions as a result of the presence of multiple species in solution with similar coordination environments. The mercury strongly prefers binding to picolinic acid over the sulfur backbone in all three structures, possibly due to their strong electrostatic attraction and decreased steric torsion, which would be required to introduce additional macrocyclic sulfur atoms into the Hg^{2+} coordination sphere.

Radiolabeling

[$^{197m/g}$Hg]Hg^{2+} concentration-dependent radiolabeling experiments with the novel sulfur-rich derivatives (**N_2S_4-Py**, **N_2S_4-Thio** and **N_2S_4-Pa^{2-}**) were conducted at both 80 °C and 25 °C (1 h incubation time, Fig. 6) at pH 7 in 1 M NH_4OAc. The results were compared to our previously reported **NS_4-BA** chelator, which exhibited the highest radiomercury incorporation yields for a chelator reported to date.[10] While both **N_2S_4-Py** and **N_2S_4-Thio** demonstrated quantitative incorporation yields (>95%) at 10^{-4} M, **N_2S_4-Pa^{2-}** was only able to achieve a radiochemical yield (RCY) of 26 ± 1% at the same concentration. At 10^{-5} M ligand concentrations, **N_2S_4-Py** maintained a high RCY of 86 ± 2%, while **N_2S_4-Thio** dropped to 65 ± 5%. However, at final ligand conditions of 10^{-6} M and 10^{-7} M, labeling of **N_2S_4-Py** and **N_2S_4-Thio** was comparable exhibiting RCYs of 17 ± 7% and 12 ± 9% at 10^{-6} M and 6 ± 2% and 6 ± 1% at 10^{-7} M, respectively. Compared to the **NS_4-BA** [$^{197m/g}$Hg]Hg-radiolabeling results, both **N_2S_4-Py** and **N_2S_4-Thio** ligands perform similarly. However, on average, **NS_4-BA** attains a slightly higher RCY at all ligand concentrations under the same conditions. At 25 °C, a dramatic decrease in the radiomercury incorporation capabilities of **N_2S_4-Py** and **N_2S_4-Pa^{2-}** was observed, resulting in an RCY of 37 ± 3% and 33 ± 0.2% at 10^{-4} M, respectively. However, **N_2S_4-Thio** at 10^{-4} M remains able to complex radio-mercury quantitatively at room temperature, followed by a sharp drop in RCY with decreasing ligand concen-

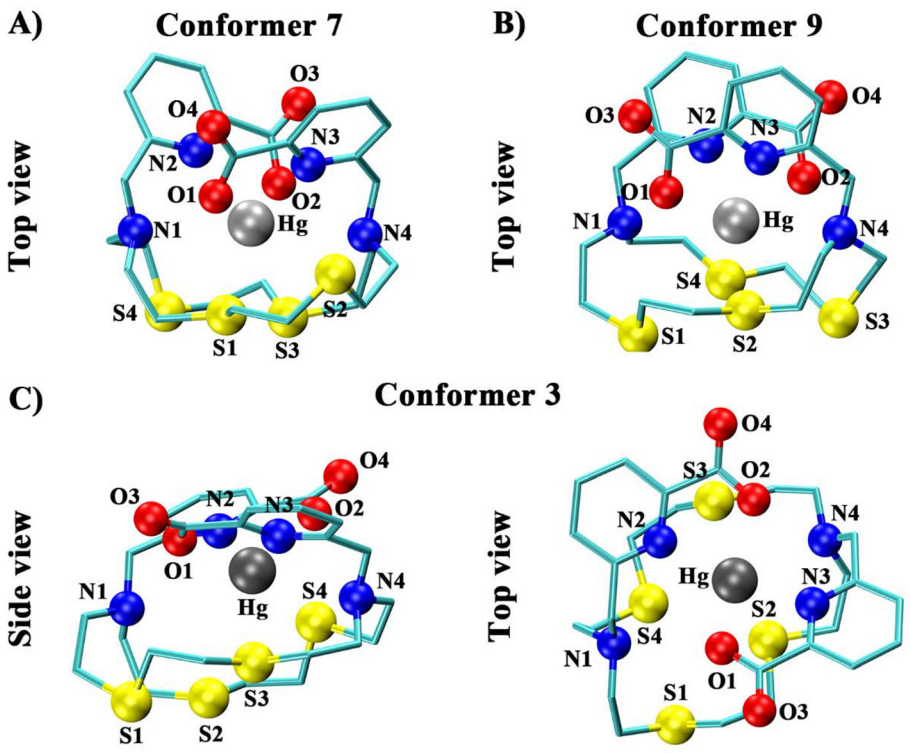

Fig. 5 B3LYP-6-311G**/SDD optimized geometries of the **(N_2S_4-Pa)$^{2-}$** Hg-complex: conformer 7 (A; ΔG_{soln} = ΔG_{gas} = 0.0 kJ mol^{-1}), conformer 9 (B; ΔG_{soln} = 1.6 kJ mol^{-1}; ΔG_{gas} = 0.6 kJ mol^{-1}), and conformer 3 (ΔG_{soln} = 3.6 kJ mol^{-1}; ΔG_{gas} = 33.6 kJ mol^{-1}) (C). Hydrogen atoms were omitted for clarity.

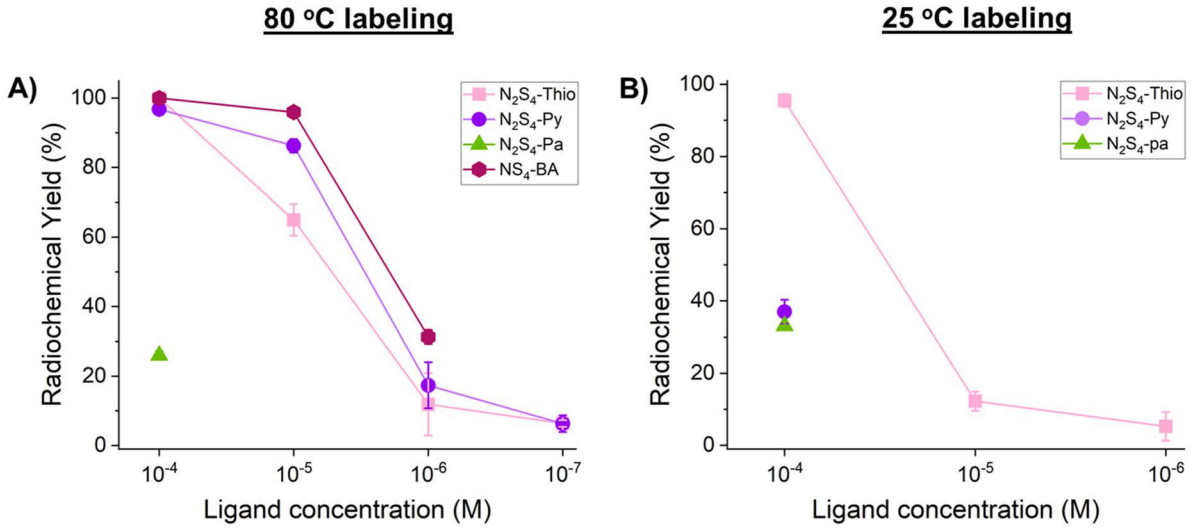

Fig. 6 Non-isolated radiochemical yields (RCYs) for [$^{197m/g}$Hg]$HgCl_2$ (~1 MBq) radiolabeling of **N_2S_4-Py**, **N_2S_4-Thio** and **N_2S_4-Pa^{2-}** (1 M NH_4OAc, pH 7), at various ligand concentrations at 80 °C (A) and 25 °C (B) (1 h reaction time, 100 μL reaction, and n = 3). [$^{197m/g}$Hg][Hg(**NS_4-BA**)]$^{2+}$ 80 °C labeling data are reproduced from Randhawa *et al.*[10]

tration (12 ± 3% and 5 ± 4% at a final ligand conc. of 10^{-5} and 10^{-6} M, respectively).

Although the complexation of Hg^{2+} with all ligands was successful at the macroscopic scale, the radiolabeling results revealed the true influence of the pendant arms on the complexation of [$^{197m/g}$Hg]Hg^{2+}. Differences in complexation at macroscopic (NMR) and microscopic (radiolabeling) scales are commonly observed and could be attributed to the trace amount of the (radio)metal at the radiolabeling scale compared to the chelator in solution (C_{ligand} = C_{metal} = ~10^{-2} M for NMR, *vs.* C_{ligand} = ~10^{-3}–10^{-7} M and $C_{radiometal}$ = ~10^{-9} M in radiolabeling studies). General trends demonstrated that increasing the softness of the pendant arms increases the ligand's ability to complex [$^{197m/g}$Hg]Hg^{2+}. The decrease seen in the RCY of **N_2S_4-Py** at 25 °C may be a result of the activation barrier of complex formation due to the bulkiness of the pendant arms. Interestingly, the ligand derivative with picolinic acid pendant arms did not yield qualitative radiolabeling under any conditions studied, regardless of the strong electrostatic interactions provided by the carboxylic acids—the trend suggesting that the principle of Pearson's HSAB theory heavily impacts the ability of the ligand to complex [$^{197m/g}$Hg]Hg^{2+} and that **N_2S_4-Pa^{2-}** is not a suitable chelator for $^{197m/g}$Hg-radiopharmaceutical development. However, the low RCY can also be attributed to the known affinity of **N_2S_4-Pa^{2-}** to form metal ion complexes with other intermediate metals (*e.g.* Bi^{3+} and In^{3+}), and any non-radioactive metal impurities in the radiolabeling mixtures may significantly compete for radio-Hg complexation.

Kinetic inertness of radiolabeled complexes

Developing kinetically inert ligands for Hg^{2+} complexation is challenging due to the labile nature of the cation. The *in vitro* kinetic inertness of the [$^{197m/g}$Hg][**Hg(N_2S_4-Py)**]$^{2+}$ and [$^{197m/g}$Hg][**Hg(N_2S_4-Thio)**]$^{2+}$ complexes was assessed against human serum, L-glutathione (GSH) and stable biologically relevant metals ($ZnCl_2$, $FeCl_3$, $CuCl_2$, $MgCl_2$ and $CoCl_2$) over time (Fig. 7). The kinetic inertness of the radio-mercery complexes against endogenous proteins found in human serum at 37 °C over 72 h was determined *via* sodium dodecyl sulfate-polyacrylamide gel electrophoresis (SDS-PAGE) using previously established procedures.[8,10] Within 1 h of incubation with human serum, both [$^{197m/g}$Hg][**Hg(N_2S_4-Py)**]$^{2+}$ and [$^{197m/g}$Hg][**Hg(N_2S_4-Thio)**]$^{2+}$ had significantly dissociated resulting in 71 ± 1% and 76 ± 2% intact complex remaining, respectively. After the initial drop in the intact complex, the rate of transchelation decreased dramatically over the 72 h incubation period culminating with 65 ± 2% and 60 ± 2% intact complex remaining for [$^{197m/g}$Hg][**Hg(N_2S_4-Py)**]$^{2+}$ and [$^{197m/g}$Hg][**Hg(N_2S_4-Thio)**]$^{2+}$, respectively. Compared to our previously reported [$^{197m/g}$Hg]Hg-**NS_4-BA** complex, both N_2S_4 complexes were relatively less inert over the investigated timeframe (24 h).

Kinetic stability was also assessed against GSH, as the most abundant thiol-containing small molecule in mammalian cells (millimolar concentrations), with a known affinity for Hg^{2+}. GSH was incubated with the [$^{197m/g}$Hg]Hg^{2+}-complexes so that the final concentration would mimic *in vivo* within cell concentrations (2.12 mM)[35] at 37 °C, and complex inertness was analyzed over 24 h by radio-iTLC. [$^{197m/g}$Hg][**Hg(N_2S_4-Py)**]$^{2+}$ and [$^{197m/g}$Hg][**Hg(N_2S_4-Thio)**]$^{2+}$ remained 86 ± 0.4% and 78 ± 0.4% intact over 1 h, and 73 ± 0.4% and 75 ± 3% intact over 3 h, respectively. However, after 24 h, the complex integrity diminished to 32 ± 5% for [$^{197m/g}$Hg][**Hg(N_2S_4-Py)**]$^{2+}$ and 44 ± 3% for [$^{197m/g}$Hg][**Hg(N_2S_4-Thio)**]$^{2+}$. Both $^{197m/g}$Hg-labeled N_2S_4 derivatives were significantly less inert in GSH compared to the previously reported $^{197m/g}$Hg-**NS_4-BA** complex, which remained ~90% intact over 3 days.[10]

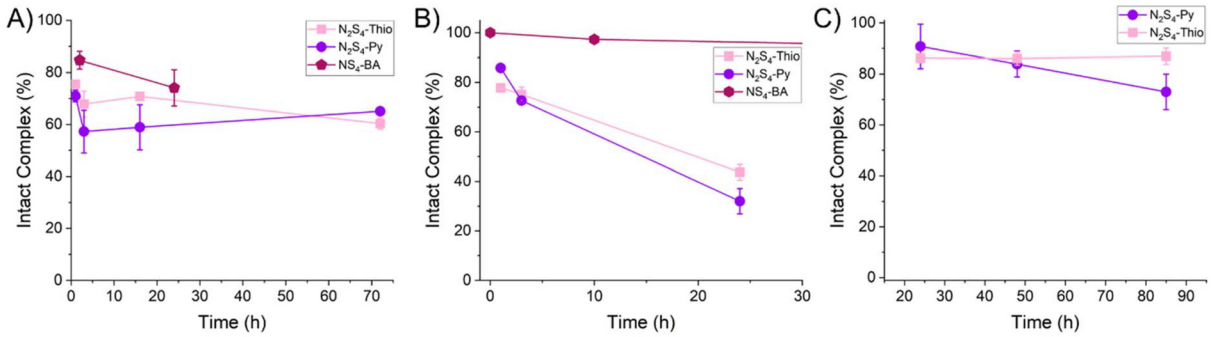

Fig. 7 Kinetic inertness of [$^{197m/g}$Hg][**Hg(N_2S_4-Py)**]$^{2+}$ and [$^{197m/g}$Hg][**Hg(N_2S_4-Thio)**]$^{2+}$ against (A) human serum, (B) glutathione with comparison to the formerly reported **NS_4-BA** and (C) stable biologically relevant metals ($ZnCl_2$, $FeCl_3$, $CuCl_2$, $MgCl_2$ and $CoCl_2$) at 37 °C (n = 3) over time. [$^{197m/g}$Hg][Hg(**NS_4-BA**)]$^{2+}$ stability data are reproduced from Randhawa *et al.*[10]

The kinetic inertness of the [$^{197m/g}$Hg][**Hg(N_2S_4-Py)**]$^{2+}$ and [$^{197m/g}$Hg][**Hg(N_2S_4-Thio)**]$^{2+}$ complexes against a mixture of biologically relevant metals ($ZnCl_2$, $FeCl_3$, $CuCl_2$, $MgCl_2$ and $CoCl_2$), which were added in a 10-fold excess compared to the ligand and 10^6-fold excess compared to the radiometal, was assessed. The reaction was incubated at 25 °C and monitored by radio-iTLC for over 82 h. [$^{197m/g}$Hg][**Hg(N_2S_4-Thio)**]$^{2+}$ remained 86 ± 3% intact, while [$^{197m/g}$Hg][**Hg(N_2S_4-Py)**]$^{2+}$ remained 73 ± 7% intact at 82 h. The relatively high inertness of the Hg-complexes in this metal competition assay is not surprising due to the ligand backbone's high selectivity for Hg^{2+} compared to other metals, as demonstrated in the literature.[11]

Throughout all three kinetic inertness assays performed, both [$^{197m/g}$Hg][**Hg(N_2S_4-Py)**]$^{2+}$ and [$^{197m/g}$Hg][**Hg(N_2S_4-Thio)**]$^{2+}$ performed similarly, suggesting that their pendant arms do not play a significant role in altering the relative inertness of the resulting $^{197m/g}$Hg-complex. However, both complexes exhibited inferior kinetic inertness compared to that of the [$^{197m/g}$Hg][Hg(**NS_4-BA**)]$^{2+}$ complex.

Conclusion

This work illustrates the effects of both the softness of pendant arm donor atoms and the macrocyclic ring size on [$^{197m/g}$Hg]Hg^{2+} radiolabeling and complex stability. Following the synthesis and characterization of the N_2S_4 ligand series, Hg^{2+} complexes were studied through mass spectrometry, nuclear magnetic resonance (NMR) spectroscopy, and density functional theory (DFT) calculations, investigating the impact of the donor atoms and ring size on the metal coordination chemistry. NMR revealed successful complexation of the Hg^{2+} ion, suggested by the broadening and downfield shifting of proton resonances close to donor atoms involved in metal coordination. Furthermore, DFT calculations supported the coordination observed *via* NMR. The lowest energy conformations yielded pendant arms in the *cis* geometry for all complexes. **[Hg(N_2S_4-Thio)]$^{2+}$** resulted in a 5-coordinate complex (distorted trigonal pyramidal), while both **[Hg(N_2S_4-Py)]$^{2+}$** and **[Hg(N_2S_4-Pa)]** resulted in a 6-coordinate complex with the distorted octahedral arrangement in solution. The DFT calculations displayed the solvation effect influence on the lowest energy conformation and further uncovered the impact of the ring size on metal coordination. The ability of all the donor atoms in the backbone to interact with the Hg^{2+} metal atom simultaneously was found to be highly thermodynamically unfavorable due to significant steric strain on the backbone, due to the larger ring size. Within the **[Hg(N_2S_4-Thio)]$^{2+}$** and **[Hg(N_2S_4-Py)]$^{2+}$** computed structures, the metal is situated asymmetrically in the ligand backbone, resulting in a highly asymmetric complex, as seen by NMR. However, the **[Hg(N_2S_4-Pa)]** complex attains strong coordination between the picolinic acid donor arms because of their electrostatic interactions; the calculations revealed 3 low energy conformers with the same coordination sphere, which agrees with the NMR data. Moreover, radiolabeling studies confirmed the true trends in the pendant arm effect on [$^{197m/g}$Hg]Hg^{2+} coordination demonstrating that the soft thioether pendant arms have the highest affinity for [$^{197m/g}$Hg]Hg^{2+}, followed by the pyridine arms. The [$^{197m/g}$Hg][**Hg(N_2S_4-Py)**]$^{2+}$ and [$^{197m/g}$Hg][**Hg(N_2S_4-Thio)**]$^{2+}$ complexes remained above 60% intact over 72 h when incubated in human serum and above 30% intact over 24 h when incubated in GSH, respectively. Notably, the kinetic inertness of the N_2S_4 complexes was inferior compared to the previously reported [$^{197m/g}$Hg][Hg(**NS_4-BA**)]$^{2+}$ complex. The [$^{197m/g}$Hg][**Hg(N_2S_4-Py)**]$^{2+}$ and [$^{197m/g}$Hg][**Hg(N_2S_4-Thio)**]$^{2+}$ complex integrity was also tested against biologically relevant metals ($ZnCl_2$, $FeCl_3$, $CuCl_2$, $MgCl_2$ and $CoCl_2$) at 37 °C, in which they remained above 73% intact over 82 h, suggesting selectivity of the ligands for Hg^{2+}. Although the N_2S_4 ligand series demonstrates selective labeling for radio-Hg at both 80 and 25 °C, the complex stability was relatively poor compared to the [$^{197m/g}$Hg][Hg(**NS_4-BA**)]$^{2+}$ complex. The results suggest that the future development of [$^{197m/g}$Hg]Hg^{2+} bifunctional chelators should concentrate on the smaller 15-membered ring scaffold for radiopharmaceutical incorporation. Although the N_2S_4 series is not optimal for [$^{197m/g}$Hg]Hg^{2+}, these chelators may be suitable for larger soft radiometals such as [^{111}Ag]Ag^+, [^{199}Au]Au^+ and [^{201}Tl]Tl^+.

Author contributions

P. R.: conceptualization, data curation, formal analysis, investigation, methodology, visualization, and writing – original draft. C. M. K. S.: formal analysis, investigation, methodology, visualization, and writing – review and editing. S. C.: investigation, writing – review and editing. Y. G.: investigation, writing – review and editing. G. S.: funding acquisition, resources, supervision, and writing – review and editing. V. R.: resources, supervision, and writing – review and editing. C. R.: conceptualization, funding acquisition, methodology, project administration, resources, supervision, and writing – review and editing.

Data availability

The data supporting this article have been included as part of the ESI.†

Conflicts of interest

There are no conflicts of interest to declare.

Acknowledgements

Funding for this work was provided by the Natural Sciences and Engineering Research Council of Canada (NSERC) Discovery programs [grant numbers RGPIN-2019-07207 (CR), RGPIN-2018-04997 (VR), and RGPIN-2023-04922 (GS)], the Canadian Cancer Society Research Institute (CCSRI) [grant number 706774] and the Canadian Institutes of Health Research (CIHR) [grant number: GR021373]. TRIUMF received federal funding *via* a contribution agreement with the National Research Council of Canada. We thank Dr Karthika J. Kadassery and Dr Justin J. Wilson (Cornell University) for providing **N_2S_4-H_2Pa** and for their helpful and insightful discussions. We would also like to thank the TR-13 Cyclotron Operations Group consisting of Toni Epp, Ryley Morgan, and Spencer Staiger and led by David Prevost for regular irradiation of Au targets. Prof. Raymond Reilly, Dr Zhongli Cai, and the team (University of Toronto) are kindly acknowledged for their collaborative discussions.

References

1 M. Walther, S. Preusche, S. Bartel, G. Wunderlich, R. Freudenberg, J. Steinbach and H. J. Pietzsch, Theranostic Mercury: $^{197(m)}$Hg with High Specific Activity for Imaging and Therapy, *Appl. Radiat. Isot.*, 2015, **97**, 177–181, DOI: **10.1016/j.apradiso.2015.01.001**.

2 P. Randhawa, A. P. Olson, S. Chen, K. L. Gower-fry, C. Hoehr, J. W. Engle, C. F. Ramogida and V. Radchenko, Meitner-Auger Electron Emitters for Targeted Radionuclide Therapy: Antimony-119 and Mercury-197m/g, *Curr. Radiopharm.*, 2021, **14**(1), 1–26.

3 D. Filosofov, E. Kurakina and V. Radchenko, Potent Candidates for Targeted Auger Therapy: Production and Radiochemical Considerations, *Nucl. Med. Biol.*, 2021, **94–95**, 1–19, DOI: **10.1016/j.nucmedbio.2020.12.001**.

4 J. Bolcaen, M. A. Gizawy, S. Y. A. Terry, A. Paulo, B. Cornelissen, A. Korde, J. Engle, V. Radchenko and R. W. Howell, Marshalling the Potential of Auger Electron Radiopharmaceutical Therapy, *J. Nucl. Med.*, 2023, **64**(9), 1344–1351, DOI: **10.2967/jnumed.122.265039**.

5 E. W. Price and C. Orvig, Matching Chelators to Radiometals for Radiopharmaceuticals, *Chem. Soc. Rev.*, 2014, **43**(1), 260–290, DOI: **10.1039/c3cs60304k**.

6 C. F. Ramogida and C. Orvig, Tumour Targeting with Radiometals for Diagnosis and Therapy, *Chem. Commun.*, 2013, **49**(42), 4720–4739, DOI: **10.1039/c3cc41554f**.

7 R. Freudenberg, R. Apolle, M. Walther, H. Hartmann and J. Kotzerke, Molecular Imaging Using the Theranostic Agent $^{197(m)}$Hg: Phantom Measurements and Monte Carlo Simulations, *EJNMMI Phys.*, 2018, **5**(1), 1–14, DOI: **10.1186/s40658-018-0216-9**.

8 P. Randhawa, I. Carbo-Bague, P. R. W. J. Davey, S. Chen, H. Merkens, C. F. Uribe, C. Zhang, M. Tosato, F. Bénard, V. Radchenko and C. F. Ramogida, Exploration of Commercial Cyclen-Based Chelators for Mercury-197m/g Incorporation into Theranostic Radiopharmaceuticals, *Front. Chem.*, 2024, **12**, 1292566, DOI: **10.3389/fchem.2024.1292566**.

9 R. G. Pearson, Hard and Soft Acids and Bases. HSAB, Part 1: Fundamentals Principles, *J. Chem. Educ.*, 1986, **45**, 581–587.

10 P. Randhawa, K. L. Gower-Fry, C. M. K. Stienstra, M. Tosato, S. Chen, Y. Gao, A. W. McDonagh, V. Di Marco, V. Radchenko, G. Schreckenbach and C. F. Ramogida, Selective Chelation of the Exotic Meitner–Auger Emitter Mercury–197m/g with Sulfur–Rich Macrocyclic Ligands: Towards the Future of Theranostic Radiopharmaceuticals, *Chem. – Eur. J.*, 2023, **29**(21), e202203815, DOI: **10.1002/chem.202203815**.

11 M. L. Ho, K. Y. Chen, G. H. Lee, Y. C. Chen, C. C. Wang, J. F. Lee, W. C. Chung and P. T. Chou, Mercury(II) Recognition and Fluorescence Imaging in Vitro through a 3D-Complexation Structure, *Inorg. Chem.*, 2009, **48**(21), 10304–10311, DOI: **10.1021/ic901613s**.

12 P. Randhawa, K. J. Kadassery, B. L. McNeil, S. N. MacMillan, L. Wharton, H. Yang, J. J. Wilson and C. F. Ramogida, The H_2S_XMacropa Series: Increasing the Chemical Softness of H_2Macropa with Sulfur Atoms to Chelate Radiometals $[^{213}Bi]Bi^{3+}$ and $[^{203}Pb]Pb^{2+}$ for Radiopharmaceutical Applications, *Inorg. Chem.*, 2024, DOI: **10.1021/acs.inorgchem.4c03498**.

13 M. Tosato, M. Asti, M. Dalla Tiezza, L. Orian, D. Häussinger, R. Vogel, U. Köster, M. Jensen, A. Andrighetto, P. Pastore and V. D. Marco, Highly Stable Silver(I) Complexes with Cyclen-Based Ligands Bearing

Sulfide Arms: A Step Toward Silver-111 Labeled Radiopharmaceuticals, *Inorg. Chem.*, 2020, **59**(15), 10907–10919, DOI: **10.1021/acs.inorgchem.0c01405**.

14 M. Tosato, M. Verona, R. Doro, M. Dalla Tiezza, L. Orian, A. Andrighetto, P. Pastore, G. Marzaro and V. Di Marco, Toward Novel Sulphur-Containing Derivatives of Tetraazacyclododecane: Synthesis, Acid-Base Properties, Spectroscopic Characterization, DFT Calculations, and Cadmium(II) Complex Formation in Aqueous Solution, *New J. Chem.*, 2020, **44**(20), 8337–8350, DOI: **10.1039/d0nj00310g**.

15 M. Tosato, P. Randhawa, L. Lazzari, B. L. McNeil, M. Dalla Tiezza, G. Zanoni, F. Mancin, L. Orian, C. F. Ramogida and V. Di Marco, Tuning the Softness of the Pendant Arms and the Polyazamacrocyclic Backbone to Chelate the ^{203}Pb/^{212}Pb Theranostic Pair, *Inorg. Chem.*, 2024, **63**(4), 1745–1758, DOI: **10.1021/acs.inorgchem.3c02610**.

16 H. Yang, F. Gao, B. McNeil, C. Zhang, Z. Yuan, S. Zeisler, J. Kumlin, J. Zeisler, F. Bénard, C. Ramogida and P. Schaffer, Synthesis of DOTA-Pyridine Chelates for ^{64}Cu Coordination and Radiolabeling of αMSH Peptide, *EJNMMI Radiopharmacy Chem.*, 2021, **6**(3), DOI: **10.1186/s41181-020-00119-4**.

17 B. L. McNeil, K. J. Kadassery, A. W. McDonagh, W. Zhou, P. Schaffer, J. J. Wilson and C. F. Ramogida, Evaluation of the Effect of Macrocyclic Ring Size on [^{203}Pb]Pb(II) Complex Stability in Pyridyl-Containing Chelators, *Inorg. Chem.*, 2022, **61**(25), 9638–9649, DOI: **10.1021/acs.inorgchem.2c01114**.

18 M. Tosato, S. Franchi, A. A. Isse, A. Del Vecchio, G. Zanoni, A. Alker, M. Asti, T. Gyr, V. Di Marco and H. Mäcke, Is Smaller Better? Cu^{2+}/Cu^{+} Coordination Chemistry and Copper-64 Radiochemical Investigation of a 1,4,7-Triazacyclononane-Based Sulfur-Rich Chelator, *Inorg. Chem.*, 2023, **62**(50), 20621–20633, DOI: **10.1021/acs.inorgchem.3c00621**.

19 M. Tosato, P. Randhawa, L. Lazzari, B. McNeil, C. Ramogida and V. Di Marco, Harnessing the Theranostic Potential of Lead Radioisotopes with Sulphur-Containing Macrocycles, *Nucl. Med. Biol.*, 2022, **108–109**, S158–S159, DOI: **10.1016/S0969-8051(22)00337-7**.

20 S. Chen, M. Bas, S. Happel, P. Randhawa, S. McNeil, E. Kurakina, S. Zeisler, K. Maskell, C. Hoehr, C. F. Ramogida and V. Radchenko, Determination of Distribution Coefficients of Mercury and Gold on Selected Extraction Chromatographic Resins - towards an Improved Separation Method of Mercury-197 from Proton-Irradiated Gold Targets, *J. Chromatogr., A*, 2023, **1688**, 463717, DOI: **10.1016/j.chroma.2022.463717**.

21 H. Behera, V. Ramkumar and N. Madhavan, Cation-Transporting Peptides: Scaffolds for Functionalized Pores?, *Chem. – Eur. J.*, 2015, **21**(28), 10179–10184, DOI: **10.1002/chem.201500881**.

22 H. Khanmohammadi, M. Pass, K. Rezaeian and G. Talei, Solvatochromism, Spectral Properties and Antimicrobial Activities of New Azo–Azomethine Dyes with N2S2O2 Donor Set of Atoms, *J. Mol. Struct.*, 2014, **1072**, 232–237, DOI: **10.1016/j.molstruc.2014.05.014**.

23 J. Jurczak, T. Stankiewicz, P. Sałański, S. Kasprzyk and P. Lipkowski, A New Method for the Synthesis of Diazacoronands via Double-Amidation Reaction, *Tetrahedron*, 1993, **49**(7), 1478–1488, DOI: **10.1016/S0040-4020(01)90200-5**.

24 D. M. Weekes, C. F. Ramogida, M. D. G. Jaraquemada-Peláez, B. O. Patrick, C. Apte, T. I. Kostelnik, J. F. Cawthray, L. Murphy and C. Orvig, Dipicolinate Complexes of Gallium(III) and Lanthanum(III), *Inorg. Chem.*, 2016, **55**(24), 12544–12558, DOI: **10.1021/acs.inorgchem.6b02357**.

25 M. K. Frisch, G. W. Trucks, H. B. Schegel, G. E. Scuseria, M. A. Robb, G. A. Cheeseman and H. Nakatsuji, *Gaussian 16*, 2016.

26 A. D. Becke, Density-Functional Thermochemistry. III. The Role of Exact Exchange, *J. Chem. Phys.*, 1993, **98**(7), 5648–5652, DOI: **10.1063/1.464913**.

27 T. Lecklider, Maintainng a Heathy Rhythm, *Eval. Eng.*, 2011, **50**(11), 36–39.

28 A. D. Becke and E. R. Johnson, A Density-Functional Model of the Dispersion Interaction, *J. Chem. Phys.*, 2005, **123**, 154101, DOI: **10.1063/1.2065267**.

29 S. Grimme, J. Antony, S. Ehrlich and H. Krieg, A Consistent and Accurate Ab Initio Parametrization of Density Functional Dispersion Correction (DFT-D) for the 94 Elements H-Pu, *J. Chem. Phys.*, 2010, **132**, 154104, DOI: **10.1063/1.3382344**.

30 D. Andrae, U. Häußermann, M. Dolg, H. Stoll and H. Preuß, Energy-Adjusted Ab Initio Pseudopotentials for the Second and Third Row Transition Elements, *Theor. Chim. Acta*, 1990, **77**(2), 123–141, DOI: **10.1007/BF01114537**.

31 B. Mennucci, Polarizable Continuum Model, *Wiley Interdiscip. Rev.: Comput. Mol. Sci.*, 2012, **2**(3), 386–404, DOI: **10.1002/wcms.1086**.

32 M. D. Hanwell, D. E. Curtis, D. C. Lonie, T. Vandermeerschd, E. Zurek and G. R. Hutchison, Avogadro: An Advanced Semantic Chemical Editor, Visualization, and Analysis Platform, *J. Cheminf.*, 2012, **4**, 17, DOI: **10.1186/1758-2946-4-17**.

33 P. F. B. Gonçalves and H. Stassen, Calculation of the Free Energy of Solvation from Molecular Dynamics Simulations, *Pure Appl. Chem.*, 2004, **76**(1), 231–240, DOI: **10.1351/pac200476010231**.

34 NIST Computational Chemistry Comparison and Benchmark Database. DOI: 10.18434/T47C7Z.

35 D. A. Dickinson and H. J. Forman, Cellular Glutathione and Thiols Metabolism, *Biochem. Pharmacol.*, 2002, **64**, 1019–1026.

36 A. J. Blake, G. Reid and M. Schröder, Mercury Macrocyclic Complexes: The Synthesis of $[Hg([18]aneN_2S_4)]^{2+}$ and $[Hg(Me_2[18]aneN_2S_4)]^{2+}$, *Polyhedron*, 1990, **9**(24), 2931–2935.

37 N. Mushtaq, G. Chen, L. R. Sidra, Y. Liu and X. Fang, Synthesis and Crosslinking Study of Isomeric Poly (Thioether Ether Imide)s Containing Pendant Nitrile and

Terminal Phthalonitrile Groups, *Polym. Chem.*, 2016, **7**(48), 7427–7435, DOI: **10.1039/C6PY01705C**.

38 B. Cordero, V. Gómez, A. E. Platero-Prats, M. Revés, J. Echeverría, E. Cremades, F. Barragán and S. Alvarez, Covalent Radii Revisited, *Dalton Trans.*, 2008, (21), 2832, DOI: **10.1039/b801115j**.

39 S. Grimme, Exploration of Chemical Compound, Conformer, and Reaction Space with Meta-Dynamics Simulations Based on Tight-Binding Quantum Chemical Calculations, *J. Chem. Theory Comput.*, 2019, **15**(5), 2847–2862, DOI: **10.1021/acs.jctc.9b00143**.

40 F. P. Hinz and D. W. Margerum, Ligand Solvation and the Macrocyclic Effect. Nickel(II)-Tetramine Complexes, *Inorg. Chem.*, 1974, **13**(12), 2941–2949, DOI: **10.1021/ic50142a032**.

41 A. Y. Li, H. B. Ji and L. J. Cao, Theoretical Study on Effects of Hydrogen Bonding on the Ring Stretching Modes of Pyridine, *J. Chem. Phys.*, 2009, **131**(16), 164305, DOI: **10.1063/1.3251123**.

42 C. Tanford, *The Hydrophobic Effect: Formation of Micelles and Biological Membranes*, Wiley-Interscience Publication, New York, 2nd edn, 1973.